ACS APPLIED MATERIALS & INTERFACES

Research Article

www.acsami.org

Highly Ordered Mesoporous TiO_2–Fe_2O_3 Mixed Oxide Synthesized by Sol–Gel Pathway: An Efficient and Reusable Heterogeneous Catalyst for Dehalogenation Reaction

Astam K. Patra, Arghya Dutta, and Asim Bhaumik*

Department of Materials Science, Indian Association for the Cultivation of Science, Jadavpur, Kolkata–700032, India

Supporting Information

ABSTRACT: Highly ordered two-dimensional (2D) hexagonal TiO_2–Fe_2O_3 mixed-oxide material MFT-1, which is composed of very tiny nanoparticles, is synthesized using sodium dodecylsulfate (SDS) as a structure-directing agent. Interestingly, synthesis of an ordered mesophase was not possible using SDS as a template for mesoporous pure Fe_2O_3 or TiO_2 phases. This mesoporous iron–titanium mixed-oxide material has been characterized by powder X-ray diffraction (XRD), field-emission scanning electron microscopy (FESEM), high-resolution transmission electron microscopy (HRTEM), N_2 sorption, ultraviolet–visible light diffuse reflectance spectroscopy (UV–vis DRS) studies. N_2 sorption analysis revealed high surface areas (126–385 $m^2\ g^{-1}$) and narrow pore size distributions (3.1–3.4 nm) for different samples. UV–vis DRS spectra and wide-angle powder XRD patterns indicate that the material is composed of α-Fe_2O_3 and anatase TiO_2 phases. This TiO_2–Fe_2O_3 mixed-oxide material can act as a very efficient and reusable catalyst in the dehalogenation of aromatic chloride-, bromide-, and iodide-tolerating –F, –CN, $-CH_3$, $-OCH_3$ and $-NO_2$ functional groups in the aromatic ring using 2-propanol as the dispersion medium.

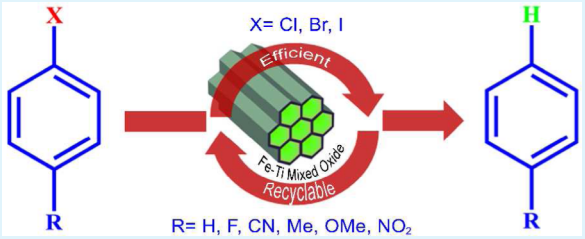

KEYWORDS: *ordered mesoporous materials, iron–titanium mixed oxide, heterogeneous catalysis, recycling efficiency, dehalogenation*

INTRODUCTION

Mesoporous metal oxides and mixed-metal oxides have been receiving considerable attention in the recent years, because of their excellent surface properties, such as high BET surface area, large pore volume, and well-organized pore channels constituted by the network elements. These materials can be utilized in wide range of applications covering gas adsorption,[1] sensing,[2] catalysis,[3−6] removal of hazardous ions,[7,8] optoelectronics,[9,10] sustainable energy,[11,12] and so on. These materials are remarkably active as catalysts for various organic transformations, such as acid-[13,14] or base-catalyzed reactions,[15,16] redox reactions,[17,18] and size- and shape-selective isomerization.[19] The well-ordered mesopores and the high surface area of these materials permit the organic molecules to access the active sites without facing much of the diffusional restrictions.

Aromatic and aliphatic halogenated compounds are one of the most important molecules in fine chemical synthesis and pharmaceutical industries. The halogen atoms in these molecules play a very crucial role in directing, substituting, and blocking some positions in the aromatic ring.[20−22] These compounds are inexpensive and are used extensively in the industrial process as well as in some daily needs, such as the dry cleaning of clothes, pesticides, etc.[23,24] Since these compounds are used on a wide scale, their disposal causes large accumulation of halogenated aromatics in our environment. Furthermore, some of these halogenated organic wastes that are produced in the chemical industry cause various health problems.[25−27] The Environmental Protection Agency (EPA) and the Food and Drug Administration (FDA) found that these organic wastes of halogenated aromatic compounds have some toxic effect on our ecosystem and health.[13] Thus, an efficient method for the removal of these halogenated compounds is highly demanding, from an environmental perspective. These halogenated aromatic compounds were generally decomposed through ignition in earlier days. However, this process produced a large amount of greenhouse gas carbon dioxide (CO_2). Scientists then discovered that some biological enzymes have dehalogenation activity.[28−30] However, these biodegradation methods were found to be unsuccessful for wide-scale applications. In addition, we cannot recover and reuse aromatic rings of halogenated aromatic compounds, while following these decomposition methods. So the dehalogenation of halogenated aromatic compounds are studied at laboratory-scale intensively over many catalysts such as Pd/Au,[31−34] transition metals,[35−38] phosphinorhodium catalyst,[39] or through photochemical reactions.[40] Recently, Wangelin et al. have reported that $Fe(acac)_3$ and commercial *t*-BuMgCl as a effective dehalologenation catalyst with very short reaction time at a temperature of 273 K.[41] However, these homogeneous

Received: July 20, 2012
Accepted: August 31, 2012
Published: August 31, 2012

   dx.doi.org/10.1021/am301394u | ACS Appl. Mater. Interfaces 2012, 4, 5022–5028

catalysts cannot be reused for several cycles and, thus, are industrially unattractive.

In this context, iron-containing catalysts have attracted particular attention,[42,43] since it is quite inexpensive and abundant, compared to late-transition metals, and it is less harmful to the environment. Furthermore, iron(III) is a harder Lewis acid, compared to late-transition-metal cations, allowing better activation of carbon halide bonds.[44] Among different approaches for heterogenization, stabilization and incorporation of an active metal into insoluble microporous[45] and mesoporous inorganic solids[3,46] having high surface areas are extensively studied. Thus, we have chosen the iron-containing, highly ordered, mesoporous materials with high surface area, good pore wall stability, as well as good mechanical, thermal, and chemical stability, which can be utilized in the dehalogenation reaction. We have developed a new highly ordered mesoporous TiO_2–Fe_2O_3 mixed oxide as a heterogeneous and reusable catalyst for dehalogenation of various aryl halides under mild conditions (see Scheme 1).

Scheme 1. Dehalogenation Reaction Using Ordered Iron–Titanium Mixed-Oxide Materials

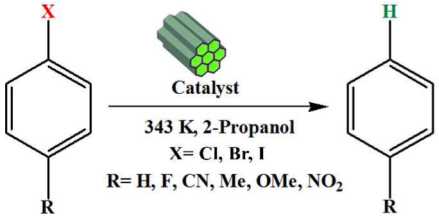

Herein, we first report a novel synthetic strategy for highly ordered two-dimensional (2D) hexagonal anatase TiO_2–α-Fe_2O_3 mixed-oxide materials using sodium dodecyl sulfate (SDS) as the structure-directing agent.

The materials were characterized by X-ray diffraction (XRD), field-emission scanning electron microscopy (FESEM), and high-resolution transmission electron microscopy (HRTEM) studies. N_2 adsorption–desorption studies showed high surface area (126–385 $m^2\ g^{-1}$) and narrow pore size distribution (3.1–3.4 nm) for the materials. The mesoporous iron–titanium mixed-oxide material was determined to be a very efficient and reusable catalyst for the dehalogenation of chloride, bromide, and iodide from the respective aromatic hydrocarbons tolerating –F, –CN, $-CH_3$, $-OCH_3$, and $-NO_2$ functional groups in the ring using 2-propanol as the hole scavenger for this dehalogenation process.

EXPERIMENTAL SECTION

Highly ordered TiO_2–Fe_2O_3 mixed oxide was synthesized via the following procedure. First, 0.82 g of anhydrous $FeCl_3$ (Merck, 99.5%) was dissolved in 10 mL of water. The solution was stirred for ~15 min. Then, 1.44 g of sodium dodecyl sulfate (SDS, Loba Chemie) was added in the solution slowly. The resulting mixture was stirred again for 30 min. Then, 2.84 g of titanium isopropoxide ($Ti(O^iPr)_4$, Aldrich Chemical Co.) was taken in 4 g of isopropyl alcohol and this solution was slowly added to the above-mentioned premixed solution. The pH of the solution then was measured (~1.0) and the resulting solution was stirred for 3 h. The mixture then was kept under freezing conditions (277 K) for 36 h. The resultant solid was collected by filtration and the material was designated as MFT-1. The solid was dried under vacuum and next kept in the oven at a temperature of 348 K for further drying. The as-synthesized solid was calcined at 773 K for 6 h to obtain template-free mesoporous iron–titanium mixed-oxide material and it was designated as MFT-1C. The as-synthesized material was extracted with an ethanol medium containing 1 N HCl for 2 h at room temperature. This acid-extracted sample was designated as MFT-1E.

We have prepared two other samples, where only Ti and Fe precursors were used individually in the respective syntheses, keeping the rest of the experimental conditions the same. In a typical synthesis of TiO_2 sample, 1.44 g of SDS (Loba Chemie) was dissolved in 20 mL of water. The solution was stirred for ~15 min. Then, 2.84 g of titanium isopropoxide ($Ti(O^iPr)_4$, Aldrich) was taken in 4 g of isopropyl alcohol, and this solution was slowly added to the above-mentioned solution. The pH of the solution then was measured (~6.0) and the pH of the solution was adjusted to ca. 8.0 via the addition of dilute NaOH solution, and the resulting mixture was stirred for 3 h. The mixture then was kept under freezing conditions (277 K) for 36 h. For the Fe_2O_3 sample, first, 1.44 g of SDS (Loba Chemie) was dissolved in 20 mL of water. The solution was stirred for ~15 min. Then, 1.62 g of anhydrous $FeCl_3$ (Merck, 99.5%) was dissolved in 5 mL of water and added in the solution slowly. The resulting mixture was stirred again for 30 min. The pH of the solution then was measured (~1.0) and the pH of the solution was adjusted to ca. 4.0 via the addition of dilute NaOH solution, and the resulting sol was stirred for 3 h. The mixture then was kept under freezing conditions (277 K) for 36 h.

The Facile Procedure for the Dehalogenation Reaction. The dehalogenation reaction of different aromatic halides over mesoporous TiO_2–Fe_2O_3 mixed-oxide material has been carried out in a two-necked round-bottom flask fitted with a water condenser and placed in an oil bath at 343 K under vigorous stirring. For a typical reaction, 5 mmol of aromatic halide, 60 mg (0.14 mmol Fe) of the catalyst, and 2.0 mL of 2-propanol were mixed together. To understand the mechanism of this reaction, we carried out the same reaction in the presence of NaOH, which can react with HX (when X = I) and isolate the I ions formed in the reaction in the form of NaI. Therefore, the I ions released from 4-iodoanisole as sodium iodide (NaI) and precipitated from the reaction mixture because of the low solubility of NaI in 2-propanol. For all of the reactions (listed in Table 1) at the selected time intervals,, the products were collected from the reaction mixtures and analyzed using an Agilent Model 4890D capillary gas chromatography instrument equipped with a flame ionization detector (FID). The products of the reactions were identified from the known standards.

Recyclability of the Catalyst. The reusability of the mesoporous TiO_2–Fe_2O_3 mixed-oxide catalyst was examined for iodobenzene dehalogenation reaction in 2-propanol. After completion of the reaction, the catalyst was separated by simple filtration and was washed thoroughly with 2-propanol several times. For the next reaction, the catalyst was activated through drying at 343 K for 4 h and used for subsequent recycling experiments. The recycling was performed for three repetitive reaction cycles.

Characterization Technique. Powder X-ray diffraction (XRD) patterns of the samples were recorded on a Bruker Advance D-8 diffractometer operated at a voltage of 40 kV and a current of 40 mA, using Cu Kα (λ = 0.15406 nm) radiation. TEM images were recorded in a JEOL Model 2010 TEM operated at 200 kV. A JEOL Model JEM 6700F field-emission scanning electron microscopy (FESEM) system was used to determine the particle morphology. Nitrogen sorption isotherms were obtained using a Belsorp-HP surface area analyzer at 77 K. Prior to the measurement, the samples were degassed at 393 K for 12 h. Thermogravimetric analysis (TGA) and differential thermal analysis (DTA) of the sample were carried out in a TGA Instruments Model TA-SDT Q-600 thermal analyzer under air flow. Ultraviolet–visible light diffuse reflectance spectroscopy (UV-vis DRS) spectra were recorded on a Shimadzu Model UV 2401PC system with an integrating sphere attachment. $BaSO_4$ was used as background standard. The reaction mixtures of the catalytic reactions were analyzed by capillary gas chromatography (Agilent Model 4890D, using a gas chromatograph equipped with a flame ionization detection (FID) device).

Table 1. MFT-1E-Catalyzed Dehalogenation of Aromatic Halides in 2-Propanol[a]

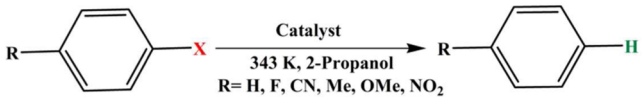

Entry	Reactant	Product	Time (h)	Conversion(%)[b]	TON[c]
1	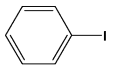		24	90	32.2
2	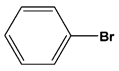		24	78	27.9
3	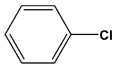		24	46	16.4
4	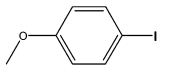	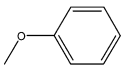	24	88	31.4
5	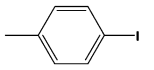	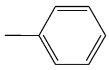	24	87	31.0
6	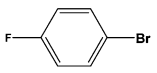	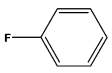	24	68	23.5
7	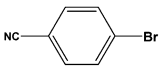	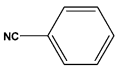	24	73	26.0
8	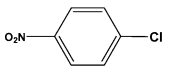	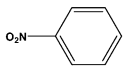	24	38	13.6
9[d]	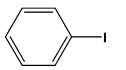		24	34	2
10[e]	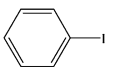		24	0	-
11[f]	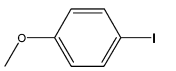	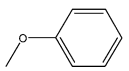	24	82	29.3

[a]Reaction condition: halogenated aromatic substrate (5 mmol), MFT-1E (60 mg, 0.14 mmol Fe), and 2 mL of 2-propanol. [b]Conversion of product calculated using gas chromatography. [c]TON (turnover number) = number of moles of substrate converted/number of moles of active site of the catalyst. [d]Reaction was carried out with $FeCl_3$ as a catalyst. [e]Reaction carried out without 2-propanol. [f]Reaction was carried out in the presence of NaOH (5 mmol).

RESULTS AND DISCUSSION

The small-angle powder X-ray diffraction (XRD) patterns for the as-synthesized MFT-1 and template-extracted sample MFT-1E are shown in Figure 1A. Both the samples show three prominent peaks in their respective powder XRD patterns, and these peaks could be assigned as the (100), (110), and (200) planes of the 2D hexagonal mesophase.[46] Unlike SDS-templated synthesis of 2D hexagonal mesophases of alumina and nickel oxides, which were accomplished in the presence of urea as the hydrolyzing agent,[47−49] here, we have not used any additional hydrolyzing agent.

The acid-extracted sample also retained the peaks and the 2D hexagonal mesophase. During acid extraction, the *d*-spacing of the hexagonal mesophase decreases. This could be attributed to the contraction of the pore wall (and *d*-spacing) during the removal of the template molecules like that observed for the conventional surfactant-templated mesoporous materials.[46−49] The wide-angle XRD pattern of the as-synthesized sample (MFT-1) and calcined sample (MFT-1C) is shown in Figure 1B. The wide-angle XRD result suggested that as-synthesized MFT-1 sample is composed of semicrystalline nanoparticles. However, upon calcination, the material became highly crystalline. The resulting XRD pattern is shown in Figure 1B, which is a mixture of anatase TiO_2 and α-Fe_2O_3 phases. Crystalline planes corresponding to the peaks for anatase TiO_2 and α-Fe_2O_3 have been indexed in this figure. Calcined sample shows major peaks at 2θ values of 25.3°, 37.8°, 48.0°, and 54.2°, which correspond to anatase TiO_2 (101), (004), (200), and (105) crystal planes (JCPDS File Card No. 21-1272).[50,51] Furthermore, major peaks at 2θ values of 33.0°, 35.4°, 40.7°, 43.4°, and 49.2° could be assigned to α-Fe_2O_3 (104), (110), (113), (202), and (024) crystal planes (JCPDS File Card No. 03-0800).[52] Thus, powder XRD results revealed that we have synthesized highly stable and crystalline TiO_2−Fe_2O_3 mixed oxide through this method, employing SDS as a templating agent. On the other hand, peaks corresponding to a layered structure were observed in the small-angle XRD pattern of pure TiO_2 sample synthesized under these conditions. However, no peaks are seen in the respective wide-angle powder XRD pattern of the pure Fe_2O_3 sample. This product was a sticky mass with no small-angle diffraction too. And in the case of the pure Fe_2O_3 sample, when we increase the pH of the synthesis

dx.doi.org/10.1021/am301394u | ACS Appl. Mater. Interfaces 2012, 4, 5022−5028

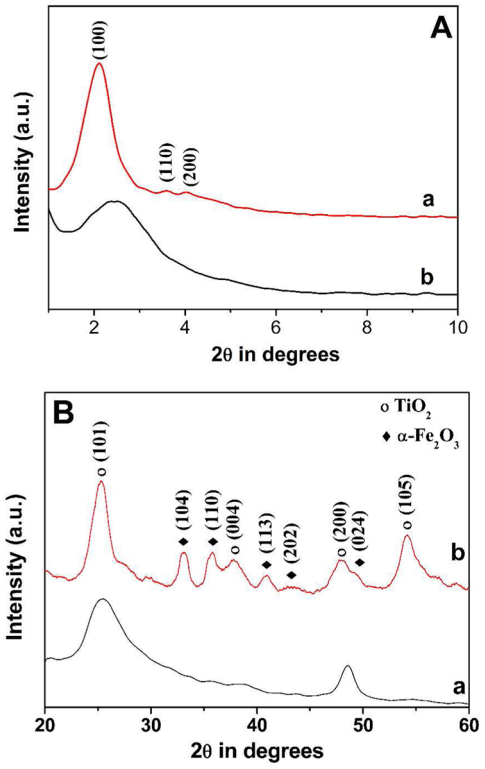

Figure 1. (A) Small-angle XRD patterns of as-synthesized MFT-1 (spectrum a) and acid ethanol extracted MFT-1E (spectrum b). (B) Wide-angle XRD patterns of as-synthesized MFT-1 (spectrum a) and calcined MFT-1C (spectrum b) ((○) anatase TiO_2 phase and (◆) α-Fe_2O_3 phase).

gel to ~4.0 by NaOH, it forms a sticky mass and with no small-angle peak. However, for the mesoporous TiO_2–Fe_2O_3 mixed-oxide synthesis, the hydrolysis of $Ti(O^iPr)_4$ is very slow, because of the very low pH (~1) of the solution. At this pH, interaction between the anionic SDS template and the cationic Fe and Ti center takes place. In the lower pH, the favorable interaction between them may stabilize the 2D hexagonal mesostructure. On the other hand, for the pure TiO_2 sample, the hydrolysis of $Ti(O^iPr)_4$ is very fast at a solution pH of ~6. At this pH, because of the presence of water, $Ti(O^iPr)_4$ hydrolyzed very fast and the interaction between SDS and Ti center takes place, leading to a layered mesostructure.

Figure 2 shows TEM image of the mesoporous TiO_2–Fe_2O_3 mixed-oxide sample. As seen from this figure, the TiO_2–Fe_2O_3 mixed oxide is composed of a highly ordered 2D hexagonal mesophase that are oriented along the [100] zone axis.[53] In this image, low-electron-density spots (pores) can be seen throughout the specimen and these are arranged in a honeycomb-like hexagonal array. The mesopores were regularly ordered, and the cavity diameter was estimated to be ~3.1 nm. The fast Fourier transform (FFT) image shown in the inset of Figure 2 indicates the 6-fold symmetry. This suggests that the prepared mesostructure is a hexagonal phase oriented along the [100] directions.[28] These textural property and particle size of the mesoporous material were further investigated via FESEM. The FESEM image (Figure 3) indicated that the sample is composed of tiny spherical nanoparticles ca. 40 nm in size, and they are self-assembled to form large spherical aggregated particles with dimensions of 120–200 nm. Chemical analysis data (using EDS) is shown in Figure S1 in the Supporting

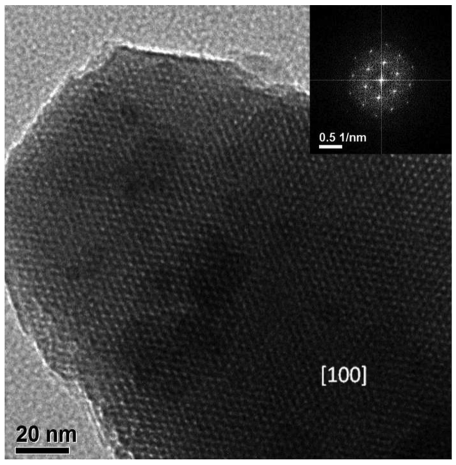

Figure 2. Representative HRTEM image of sample MFT-1, along with the [100] plane of 2D hexagonal nanostructure. A fast Fourier transform (FFT) image is shown in the inset.

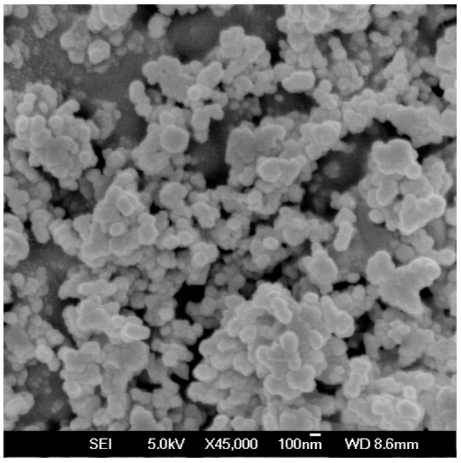

Figure 3. Representative field-emission scanning electron microscopy (FESEM) image of sample MFT-1.

Information, confirming that Fe, Ti, and O atoms are distributed uniformly in the MFT-1 material.

The N_2 adsorption–desorption isotherm of sample MFT-1E is shown in Figure 4. This isotherm could be classified as a typical Type IV isotherm characteristic of the mesoporous

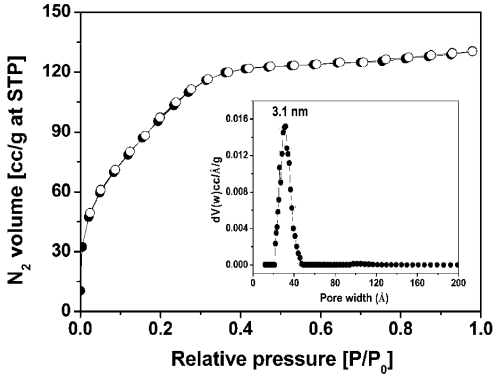

Figure 4. (●) N_2 adsorption and (○) N_2 desorption isotherms of the MFT-1E sample. The pore size distribution using the Non Local Density Functional Theory (NLDFT) Model is shown in the inset.

dx.doi.org/10.1021/am301394u | ACS Appl. Mater. Interfaces 2012, 4, 5022–5028

material.[13,14,53] In this isotherm, for a relative pressure of P/P_0 = 0.01−0.40, the adsorption amount gradually increases for the sample. However, after P/P_0 > 0.4, the N_2 uptake gets saturated. The BET surface areas for the acid-extracted (MFT-1E) and calcined samples (MFT-1C) were 385 and 126 $m^2\ g^{-1}$, respectively. Their respective pore volumes were 0.19 and 0.16 $cm^3\ g^{-1}$. Pore size distributions of these samples, employing the Non Local Density Functional Theory (NLDFT) method (using N_2 adsorption on silica as a reference),[46] suggested that the acid-extracted MFT-1E has an average pore width of ca. 3.1 nm, vis-à-vis ca. 3.4 nm for the MFT-1C sample calcined at 773 K. Pore widths obtained from this N_2 sorption analysis agree well with those values obtained independently from TEM image analysis.

The quantitative determination of the framework stability upon heat treatment of the mesoporous TiO_2−Fe_2O_3 mixed-oxide material has been studied by TGA-DTA analysis under air flow. The TGA-DTA plots are shown in Figure 5. When the

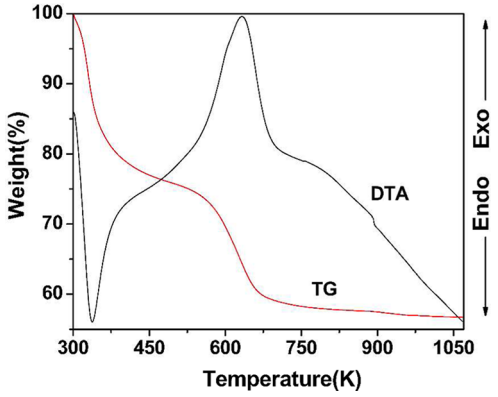

Figure 5. TG and DTA curves for as-synthesized sample MFT-1.

as-synthesized sample was heated under air, two distinct weight losses were observed. Initial weight loss could be attributed to the removal of physically adsorbed water molecules below 393 K. The gradual decrease in the weight in the temperature range of 400−685 K through one step could be attributed to the removal of organic SDS molecules present in the as-synthesized TiO_2−Fe_2O_3 mixed-oxide composite. In the temperature range of 534−700 K, a strong exothermic peak is observed in the DTA curve. This could be attributed to further condensation and dehydration to form crystalline mesoporous TiO_2−Fe_2O_3 mixed-oxide nanoparticles. Further crystallization could also take place above the temperature of 750 K.

UV−vis spectroscopy is one of the most important analytical tools for characterizing the optical properties of materials. UV−vis DRS spectra of different mesoporous TiO_2−Fe_2O_3 mixed-oxide samples are shown in Figure 6. Titania usually shows a broad absorption in the wavelength range of 300−350 nm.[46] The as-synthesized TiO_2−Fe_2O_3 mixed-oxide material showed absorption maxima at ca. 338 nm and a broad band at 484 nm. The acid-extracted material shows the same nature as that of the as-synthesized material. The UV−vis DRS spectrum of calcined MFT-1C shows an absorption band at 337 nm, as well as a broad band with a peak at 534 nm. The peak corresponding to O→Ti charge transfer in titania is observed at 337 nm, whereas the peak corresponding to 534 nm could be attributed to the d−d transition between the ground state to the excited state of Fe^{3+} present in the mixed-oxide material.[54] After calcination, the second peak is red-shifted more than as-

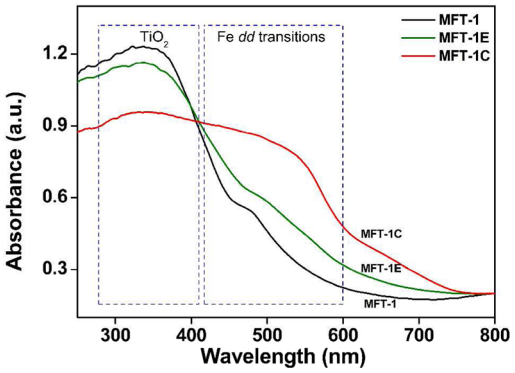

Figure 6. UV−visible diffuse reflectance spectra of samples MFT-1, MFT-1E, and MFT-1C.

synthesized material. The gradual shift in the absorption band to higher frequency region indicated the interaction between iron and titanium in the materials.[54]

Recently, iron-based catalytic systems have generated considerable interest, because iron is inexpensive and readily available as alternatives to established transition-metal-catalyzed carbon−carbon and carbon−heterobond formation reactions including different coupling reactions.[55−58] As seen from Table 1, sample MFT-1E showed high catalytic activity in dehalogenation of different aromatic halide compounds in the 2-propanol solvent.

From Table 1, we observed that conversions of 90%, 78%, and 46% take place from iodo, bromo, and chloro derivatives of halobenzene over MFT-1E under identical reaction conditions. We also performed the kinetics of these reactions (Table 1, entries 1−3), as shown in Figure S2 in the Supporting Information. This reactivity pattern could be attributed to the strength of the carbon-halide bond (Table 1, entries 1−3). Different substituted halogenated compounds are also studied, and the MFT-1E shows good catalytic activity over these reactants (Table 1, entries 4−8). To explore the potential of our new mesoporous iron−titanium mixed oxide, we have performed the same reaction with a homogeneous catalyst ($FeCl_3$). It shows very poor conversion, together with low TON value (Table 1, entry 9). It is pertinent to mention that the observed TONs, as reported in Table 1, are relatively low, because only the surface Fe center takes part in the reaction. Fe present inside the pore wall does not take part in the reaction; however, while calculating the loading of Fe, we have counted all Fe atoms present in the mixed-oxide catalyst (both surface atoms as well as those in the pore walls). Thus, consideration of higher loading of Fe decreases the TON. From this comparison, we can conclude that our mesoporous TiO_2−Fe_2O_3 mixed oxide has very good catalytic activity, because of its porous framework, which facilities the interaction between the reactant molecule and the active site of the catalyst. A probable mechanistic pathway for this halogenations reaction is shown in Figure 7. Acetone, HX (I, Br, Cl), and the corresponding aromatic compound produced in the reaction mixture. The reaction shown in Table 1 (entry 11) can be expressed by eq 1.

$$\mathrm{I{-}C_6H_4{-}OMe + (CH_3)_2CHOH + NaOH \rightarrow C_6H_5{-}OMe + (CH_3)_2CO + NaI\downarrow + H_2O} \quad (1)$$

To confirm the formation of iodide ions, NaOH was added to the reaction mixture. Iodide ions eliminated from 4-iodoanisole

dx.doi.org/10.1021/am301394u | ACS Appl. Mater. Interfaces 2012, 4, 5022−5028

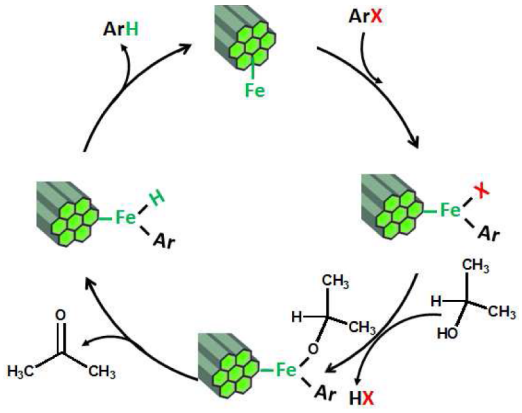

Figure 7. Proposed catalytic cycle of the reaction.

were immediately precipitated as solid NaI upon reaction with NaOH dissolved in 2-propanol. Thus, NaI could be separated from the other products of the reaction such as anisole and acetone, which are soluble in 2-propanol. Isolation of iodide from the reaction system in the form of NaI has been found to follow the stoichiometry of the dehalogenation reaction. The reusability of the mesoporous TiO_2–Fe_2O_3 mixed-oxide catalyst in the dehalogenation reaction was examined using iodobenzene as a reference, and the recycling of the catalyst was conducted for three repetitive cycles. The results are shown in Figure 8, suggesting good catalytic efficiency. We have carried

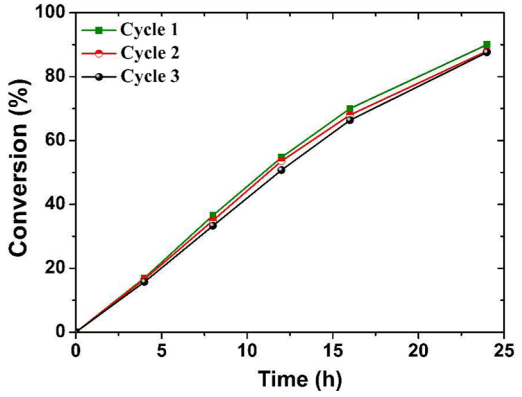

Figure 8. Recycling efficiency of the mesoporous MFT-1E catalyst with kinetics plot.

out the reaction without 2-propanol also in order to understand its role. No reaction takes place in the absence of 2-propanol (Table 1, entry 10). Here, 2-propanol acted both as a solvent and a hydrogenating agent. The 2-propanol molecule can be activated over the metal oxide surface and its dehydrogenation to acetone takes place in the reaction medium. Because of the Lewis acidic property of Fe and Ti sites present at the mesoporous TiO_2–Fe_2O_3 mixed-oxide surface, the dehydrogenation of 2-propanol could proceed smoothly.[59,60] For the photocatalytic dehalogenation, 2-propanol usually acts as a hole scavenger[61] to photogenerate electrons, which facilitates C–X (X = Cl, Br, or I) bond cleavage. On the other hand, Pd-supported-Fe_2O_3 catalyst in the presence of molecular hydrogen (H_2) also showed good catalytic dehalogenation efficiency while using 2-propanol as a solvent.[62] Thus, our experimental results suggested that ordered mesoporous TiO_2–Fe_2O_3 mixed-oxide material synthesized in the presence of a SDS template is a very efficient and recyclable catalyst in the dehalogenation of halogenated aromatics in the presence of 2-propanol as a solvent.

CONCLUSION

Highly ordered mesoporous TiO_2–Fe_2O_3 mixed oxide was successfully synthesized through a hydrothermal sol–gel synthetic approach, using an anionic surfactant as the template. This mixed-oxide mesoporous material has hexagonally ordered porous structure, high surface area, good pore wall stability, and with reactive Fe metal sites to activate the carbon–halogen bond cleavage. This mesoporous mixed-oxide material showed excellent catalytic activity in the dehalogenation of aryl iodides, bromides, and chlorides tolerating –F, –CN, $-CH_3$, $-OCH_3$, and $-NO_2$ groups in the presence of 2-propanol as a solvent. This new mesoporous catalyst remains in a separate solid phase in the reaction mixture; as a result, the recovery of the catalyst can be easily done by simple filtration and the catalyst was reused very efficiently. The unique catalytic role played by the mesoporous TiO_2–Fe_2O_3 mixed oxide may contribute significantly in environmental cleanup.

ASSOCIATED CONTENT

Supporting Information

EDS pattern of the MFT-1 material and kinetics study for the dehalogenation of the substrates (entries 1, 2, and 3 of Table 1) are provided here. This information is available free of charge via the Internet at http://pubs.acs.org/.

AUTHOR INFORMATION

Corresponding Author

*E-mail: msab@iacs.res.in.

Notes

The authors declare no competing financial interest.

ACKNOWLEDGMENTS

A.K.P. and A.D. thank CSIR, New Delhi, for their senior research fellowships. A.B. wishes to thank DST New Delhi for providing instrumental facility through the Nano Mission Initiative.

REFERENCES

(1) Choi, S.; Drese, J. H.; Jones, C. W. *ChemSusChem.* **2009**, *2*, 796–854.
(2) Pashchanka, M.; Hoffmann, R. C.; Gurlo, A.; Schneider, J. J. *J. Mater. Chem.* **2010**, *20*, 8311–8319.
(3) Corma, A. *Chem. Rev.* **1997**, *97*, 2373–2419.
(4) Tamiolakis, I.; Lykakis, I. N.; Katsoulidis, A. P.; Stratakis, M.; Armatas, G. S. *Chem. Mater.* **2011**, *23*, 4204–4211.
(5) Dutta, S.; De, S.; Patra, A. K.; Sasidharan, M.; Bhaumik, A.; Saha, B. *Appl. Catal., A* **2011**, *409*, 133–139.
(6) Wei, Z. Z.; Li, D. C.; Pang, X. Y.; Lv, C. Q.; Wang, G. C. *ChemCatChem* **2012**, *4*, 100–111.
(7) Chandra, D.; Mridha, S.; Basak, D.; Bhaumik, A. *Chem. Commun.* **2009**, 2384–2386.
(8) Patra, A. K.; Dutta, A.; Bhaumik, A. *J. Hazard. Mater.* **2012**, *201*, 170–177.
(9) Nejati, S.; Lau, K. K. S. *Nano Lett.* **2011**, *11*, 419–423.
(10) Li, Q; Zeng, L.; Wang, J.; Tang, D.; Liu, B.; Chen, G.; Wei, M. *ACS Appl. Mater. Interfaces* **2011**, *3*, 1366–1373.
(11) Ren, Y.; Hardwick, L. J.; Bruce, P. G. *Angew. Chem., Int. Ed.* **2010**, *49*, 2570–2574.
(12) Soler-Illia, G. J. A. A.; Azzaroni, O. *Chem. Soc. Rev.* **2011**, *40*, 1107–1150.

(13) Nandi, M.; Mondal, J.; Sarkar, K.; Yamauchi, Y.; Bhaumik, A. *Chem. Commun.* **2011**, *47*, 6677−6679.
(14) Khder, A. E. R. S.; Hassan, H. M. A.; El-Shall, M. S. *Appl. Catal., A* **2012**, *411*, 77−86.
(15) Fulvio, P. F.; Brosey, R. I.; Jaroniec, M. *ACS Appl. Mater. Interfaces* **2010**, *2*, 588−593.
(16) Kumar, N.; Leino, E.; Maki-Arvela, P.; Aho, A.; Kaldstrom, M.; Tuominen, M.; Laukkanen, P.; Eranen, K.; Mikkola, J.-P.; Salmi, T.; Murzin, D. Y. *Microporous Mesopororous Mater.* **2012**, *152*, 71−77.
(17) Dapurkar, S. E.; Sakthivel, A.; Selvam, P. *New J. Chem.* **2003**, *27*, 1184−1190.
(18) Dzwigaj, S.; Che, M. *Catal. Today* **2011**, *169*, 232−241.
(19) Dhakshinamoorthy, A.; Alvaro, M.; Chevreau, H.; Horcajada, P.; Devic, T.; Serre, C.; Garcia, H. *Catal. Sci. Technol.* **2012**, *2*, 324−330.
(20) Zhao, D.; Wang, W.; Yang, F.; Lan, J.; Yang, L.; Gao, G.; You, J. *Angew. Chem., Int. Ed.* **2009**, *48*, 3296−3300.
(21) Masuda, N.; Tanba, S.; Sugie, A.; Monguchi, D.; Koumura, N.; Hara, K.; Mori, A. *Org. Lett.* **2009**, *11*, 2297−2300.
(22) Liegault, B.; Petrov, I.; Gorelsky, S. I.; Fagnou, K. *J. Org. Chem.* **2010**, *75*, 1047−1060.
(23) Vogel, T. M.; Criddle, C. S.; McCarty, P. L. *Environ. Sci. Technol.* **1987**, *21*, 722−736.
(24) He, J. Z.; Ritalahti, K. M.; Yang, K. L.; Koenigsberg, S. S.; Loffler, F. E. *Nature* **2003**, *424*, 62−65.
(25) Wolf, K.; Chesnutt, T. W. *J. Hazard. Mater.* **1987**, *15*, 137−161.
(26) Townsend, G. T.; Ramanand, K.; Suflita, J. M. *Appl. Environ. Microbiol.* **1997**, *63*, 2785−2791.
(27) Tsai, W.-T. *J. Hazard. Mater.* **2011**, *190*, 1−7.
(28) Wackett, L. P. *Curr. Opin. Biotechnol.* **1994**, *5*, 260−265.
(29) Bunge, M.; Lechner, U. *Appl. Microbiol. Biotechnol.* **2009**, *84*, 429−444.
(30) Hennebel, T.; Benner, J.; Clauwaert, P.; Vanhaecke, L.; Aelterman, P.; Callebaut, R.; Boon, N.; Verstraete, W. *Biotechnol. Lett.* **2011**, *33*, 89−95.
(31) Viciu, M. S.; Grasa, G. A.; Nolan, S. P. *Organometallics* **2001**, *20*, 3607−3612.
(32) Cellier, P. P.; Spindler, J. F.; Taillefer, M.; J. Cristau, H. *Tetrahedron Lett.* **2003**, *44*, 7191−7195.
(33) Monguchi, Y.; Kume, A.; Hattori, K.; Maegawa, T.; Sajiki, H. *Tetrahedron* **2006**, *62*, 7926−7933.
(34) Hara, T.; Mori, K.; Oshiba, M.; Mizugaki, T.; Ebitani, K.; Kaneda, K. *Green Chem.* **2004**, *6*, 507−509.
(35) Matheson, L. J.; Tratnyek, P. G. *Environ. Sci. Technol.* **1994**, *28*, 2045−2053.
(36) Lipshutz, B. H.; Tomioka, T.; Sato, K. *Synlett* **2001**, 970−973.
(37) Desmarets, C.; Kuhl, S.; Schneider, R.; Fort, Y. *Organometallics* **2002**, *21*, 1554−1559.
(38) Moglie, Y.; Alonso, F.; Vitale, C.; Yus, M.; Radivoy, G. *Appl. Catal., A* **2006**, *313*, 94−100.
(39) Peterson, A. A.; Thoreson, K. A.; McNeill, K. *Organometallics* **2009**, *28*, 5982−5991.
(40) Dichiarante, V.; Fagnoni, M.; Albini, A. *Green Chem.* **2009**, *11*, 942−945.
(41) Czaplik, W. M.; Grupe, S.; Mayer, M.; von Wangelin, A. J. *Chem. Commun.* **2010**, *46*, 6350−6352.
(42) Fan, F.; Feng, Z. C.; Li, C. *Acc. Chem. Res.* **2010**, *43*, 378−387.
(43) Xuan, S.; Wang, F.; Lai, J. M. Y.; Sham, K. W. Y.; Wang, Y. X.; JLee, S. F.; Yu, J. C.; Cheng, C. H. K.; Leung, K. C. F. *ACS Appl. Mater. Interfaces* **2011**, *3*, 237−244.
(44) Gulak, S.; von Wangelin, A. J. *Angew. Chem., Int. Ed.* **2012**, *51*, 1357−1361.
(45) Sen, T.; Ramaswamy, V.; Ganapathy, S.; Rajamohanan, P. R.; Sivasanker, S. *J. Phys. Chem.* **1996**, *100*, 3809−3817.
(46) Chandra, D.; Bhaumik, A. *Ind. Eng. Chem. Res.* **2006**, *45*, 4879−4883.
(47) Yada, M.; Machida, M.; Kijima, T. *Chem. Commun.* **1996**, 769−770.
(48) Banerjee, S.; Santhanam, A.; Dhathathreyan, A.; Rao, P. M. *Langmuir* **2003**, *19*, 5522−5525.
(49) Caragheorgheopol, A.; Caldararu, H.; Vasilescu, M.; Khan, A.; Angelescu, D.; Žilkova, N.; Čejka, J. *J. Phys. Chem. B* **2004**, *108*, 7735−7743.
(50) Dong, W. Y.; Sun, Y. J.; Lee, C. W.; Hua, W. M.; Lu, X. C.; Shi, Y. F.; Zhang, S. C.; Chen, J. M.; Zhao, D. Y. *J. Am. Chem. Soc.* **2007**, *129*, 13894−13904.
(51) Patra, A. K.; Das, S. K.; Bhaumik, A. *J. Mater. Chem.* **2011**, *21*, 3925−3930.
(52) Zhan, S. H.; Chen, D. R.; Jiao, X. L.; Liu, S. S. *J. Colloid Interface Sci.* **2007**, *308*, 265−270.
(53) Fukuoka, A.; Kikkawa, I.; Sasaki, Y.; Shimojima, A.; Okubo, T. *Langmuir* **2009**, *25*, 10992−10997.
(54) Inamdar, D. Y.; Pathak, A. K.; Dubenko, I.; Ali, N.; Mahamuni, S. *J. Phys. Chem. C* **2011**, *115*, 23671−23676.
(55) Modak, A.; Mondal, J.; Sasidharan, M.; Bhaumik, A. *Green Chem.* **2011**, *13*, 1317−1341.
(56) Bolm, C.; Legros, J.; Le Paih, J.; Zani, L. *Chem. Rev.* **2004**, *104*, 6217−6254.
(57) Benfatti, F.; de Nanteuil, F.; Waser, J. *Org. Lett.* **2012**, *14*, 386−389.
(58) Paradine, S. M.; White, M. C. *J. Am. Chem. Soc.* **2012**, *134*, 2036−2039.
(59) Aramendía, M. A.; Borau, V.; Jiménez, C.; Marinas, J. M.; Porras, A.; Urbano, F. J. *J. Catal.* **1996**, *161*, 829.
(60) Klemm, L. H.; Taylor, D. R. *J. Org. Chem.* **1970**, *35*, 3216−3219.
(61) Serpone, N.; Texier, I.; Emeline, A. V.; Pichat, P.; Hidaka, H.; Zhao, J. *J. Photochem. Photobiol. A: Chem.* **2000**, *136*, 145−155.
(62) Hara, T.; Kaneta, T.; Mori, K.; Mitsudome, T.; Mizugaki, T.; Ebitani, K.; Kaneda, K. *Green Chem.* **2007**, *9*, 1246−1251.